

Coupling Mechanism of High In-Situ Stresses and High-Pressure Gases in Rockbursts of Deep Mine Roadways

ISSN: 2694-4421



*Corresponding authors: Kaiwen Zhang, China Coal Science and Engineering Group Shenyang Research Institute Co., Ltd, Shenyang, 110000, China

Submission:

☐ July 22, 2025

Published:
☐ October 28, 2025

Volume 4 - Issue 2

How to cite this article: Kaijia Zhang, Kaiwen Zhang* and Baoqiang Sun. Coupling Mechanism of High In-Situ Stresses and High-Pressure Gases in Rockbursts of Deep Mine Roadways. Academic J Eng Stud. 4(2). AES.000583.

DOI: 10.31031/AES.2025.04.000583

Copyright@ Kaiwen Zhang, This article is distributed under the terms of the Creative Commons Attribution 4.0 International License, which permits unrestricted use and redistribution provided that the original author and source are credited.

Kaijia Zhang¹, Kaiwen Zhang^{1*} and Baoqiang Sun²

¹China Coal Science and Engineering Group Shenyang Research Institute Co., Ltd, China ²China Coal Energy Research Institute Co., Ltd., China

Abstract

With the continuous increase in coal mining depth in China, dynamic disasters in coal and rock masses caused by the coexistence of high in-situ stress and high gas content have become increasingly frequent, with rockbursts being particularly typical. Taking the 1111(1) working face of the Zhuji Mine in Huainan as the engineering background, this study establishes a dual-variable coupling model of in-situ stress and gas pressure using the RFPA2D numerical simulation platform, and systematically simulates the rockburst evolution process under three typical working conditions: high stress moderate gas pressure, moderate stress-high gas pressure, and combined high stress-high gas pressure. The results show that under the combined high-stress and high-pressure condition, the initial rupture of soft coal is more intense, with the spacing between failure units reduced by 62% compared to single-factor scenarios. Large-scale collapse occurs in the upper part of the coal wall, and gas flow increases by more than 40%. The disaster-causing mechanism is characterized by the synergistic effect of stress waves generated by elastic energy release and the gas-carrying effect induced by gas desorption. Residual hard particles lead to a local stress concentration factor of up to 2.0 (compared to 1.5 in single-condition scenarios). From the perspective of energy driving, gas expansion energy increases exponentially with gas content, promoting the transition of coal movement from sliding friction to rolling friction. Frictional resistance is reduced by 38%, significantly increasing impact velocity and damage intensity. This study, for the first time, reveals the triggering mechanism of rockbursts under the coupling of high in-situ stress and high gas pressure from the perspective of energy transformation and mechanical behavior, providing theoretical guidance and technical support for the prevention and control of dynamic disasters in deep mines.

Keywords: Rockburst; High insitu stress; Gas expansion energy; Coupling mechanism; Numerical simulation

Introduction

Coal is China's primary energy source, and its dominant position in the energy mix will not change in the short term [1,2]. Most coal mines in China have entered the deep mining stage, and the number of complex dynamic disasters such as high gas content, coal and gas outbursts [3], and rockbursts is increasing. These disasters typically result from the combined effects of multiple factors and often lead to major or catastrophic mining accidents [4-6]. Most coal mines in China adopt underground mining methods, and excavation is primarily conducted through roadway development. Most rockburst incidents occur at the excavation face, where mining-induced disturbances disrupt the original equilibrium of the coal and rock mass, making dynamic disasters such as rockbursts more likely [7-9]. At present, due to the complex triggering factors and unclear disaster mechanisms of rockburst events in coal mines, coupled with increasing mining depth and intensity, the spatiotemporal characteristics of rockburst

occurrences have become more difficult to predict, severely restricting the safe and efficient exploitation of coal resources. Many scholars have conducted studies and analyses to clarify the process and mechanism of rockburst occurrences.

Cui Feng et al. [9] investigated the influence mechanism of lunarsolar tidal forces on cyclic loading and unloading of surrounding rock in mining areas, analyzed the spatiotemporal distribution of typical rockburst incidents from 2001 to 2021, and clarified the intrinsic relationship between tidal forces and rockbursts through theoretical analysis and data statistics. Askaripour et al. [10] discussed the classification and mechanisms of rockbursts, evaluated the application of current empirical methods based on geomechanical parameters for rockburst prediction, and highlighted their achievements and limitations to provide insights into deep mine risk assessment. Pan Junfeng et al. [11-13] proposed a hydraulic fracturing "artificial release layer" method to mitigate rockbursts in regions with thick, hard roofs that serve as the main disaster-inducing strata above coal seams. They also proposed dynamic and static load source differentiation methods for controlling rockbursts in deep roadways. Based on dominant controlling factors, rockbursts were categorized into three types: hard roof-dominated, geological structure-dominated, and wide coal pillar-dominated, with corresponding mitigation strategies including weakening hard roofs, redistributing highly concentrated coal pillar stress, and releasing structural stress.

Dou Linming et al. [14] proposed a coupled monitoring principle based on "stress-vibration-energy" fields for as-sessing rockburst risk and established a multi-parameter integrated monitoring and early warning system incorporat-ing stress, vibration, and energy fields. They revealed threshold laws governing energy accumulation caused by mining induced stress concentration. Dai et al. [15] proposed a quantitative evaluation model for rockburst tendency based on Geological Strength Index (GSI) and disturbance factor (D) by calculating residual elastic energy, and demonstrated its application in five tunnels. Their findings revealed that excavation disturbances reduced rockburst tendency, and that residual elastic energy and rockburst tendency were positively correlated with GSI. Zhang et al. [16], through large-scale true triaxial rockburst tests, revealed that structural plane angles and stress gradient coefficients significantly influence loading time, failure characteristics, and acoustic emission (AE) parameters.

The AE parameters in both time and frequency domains exhibited clear trends with strong potential for rockburst prediction. Wang Guifeng et al. [17] studied the unstable energy triggering mechanism of rockbursts, identified the energy thresholds for

dynamic disasters, and proposed ideas for rockburst prediction and prevention. Guo Wei et al. [18] developed an integrated system for dynamic monitoring, early warning, prevention and control, and verification of rockburst hazards, tailored to the geological and production conditions of the Cuimu Coal Mine [19]. Recent studies have shown that gas intensifies rockburst risk through dual pathways. Li Zhonghui et al. found that adsorbed gas reduces coal strength (with an elastic modulus attenuation rate >30%) and lowers critical failure stress, thereby increasing the likelihood of rockburst events.

In summary, most researchers have focused on monitoring and early warning of rockburst mechanisms and have proposed relevant theories. However, disasters occurring during coal mine operations are usually caused by a combination of factors. Although studies have been conducted separately from the perspectives of high insitu stress or high gas pressure, there is still a lack of systematic quantitative analysis of their coupled effects, particularly under extreme working conditions. This study focuses on this critical scenario by integrating insitu stress and coal seam gas pressure. Using RFPA²D software, a two-dimensional numerical model was developed based on the actual geological parameters of the Zhuji Mine in Huainan. A coupled model incorporating both stress and gas pressure was constructed with three different stress-gas scenarios to simulate the fracture evolution of coal and gas flow characteristics, and further analyze the disaster mechanism and energy transformation relationships.

Face Overview

The first mining face of Huainan Zhujii Mine 1111(1) is 1608m in strike length, 220m in inclined length, with an angle of inclination ranging from 1° to 5°, averaging at 3°. The coal seam thickness ranges from 0.1m to 2.1m, with an average of 1.2m.Roof and floor conditions: The immediate roof of the 11-2 coal seam is mudstone with an average thickness of 9.9m; the old roof consists of fine sandstone and siltstone, with an average thickness of 3.2m; the immediate floor is mudstone, with an average thickness of 4.5m; the overlying 13 coal seam has an average thickness of 4.2m, and the distance from the 11-2 coal seam is 66m (50 times the mining height); the old floor is a mix of fine sandstone and siltstone. locally containing sandy mudstone. Field measurements of the stress indicate that the vertical stress ranges from 19.3 to 20.6MPa, with the minimum horizontal principal stress being similar to the vertical stress. The lateral pressure coefficient ranges from 1.32 to 1.38, and the maximum principal stress is approximately in the east-west direction. The composite columnar section of working face is shown in Figure 1.

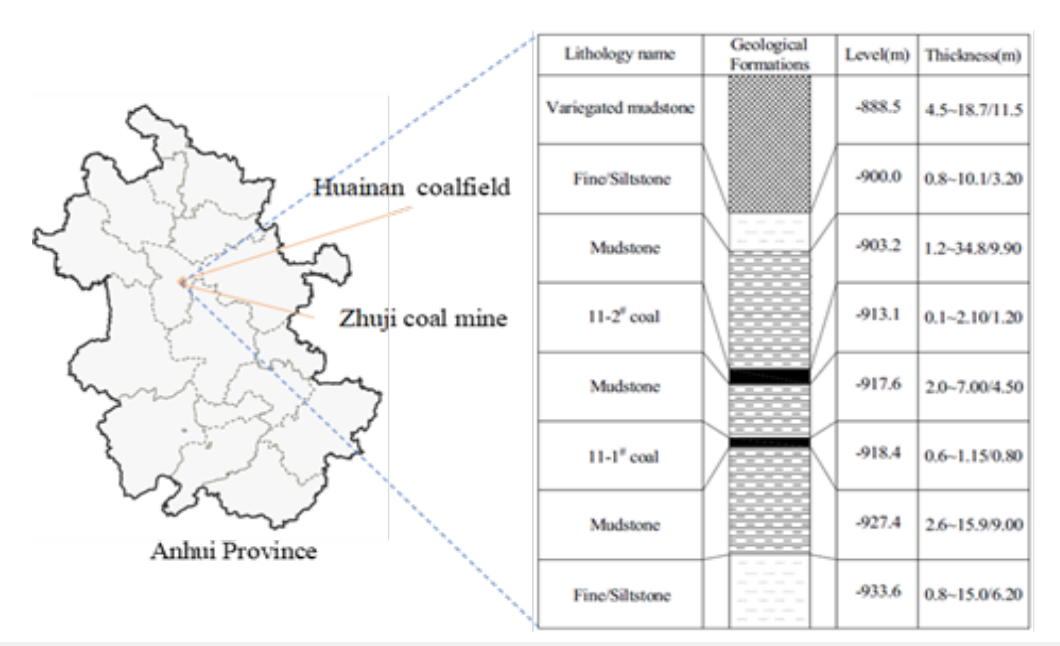


Figure 1: Borehole log for working face 1111(1) at Zhujidong coal mine, Huainan Mining (group) co., ltd., Anhui Province, China.

Numerical Simulation of Seismic Ground Pressure Triggering

Model setup

Based on the characteristics of seismic ground pressure in coal mines, it can be seen that most seismic ground pressure occurs in tunneling and mining haulage roadways. Therefore, the subject of the numerical simulation study is seismic ground pressure

in roadways, as shown in Figure 2. Figure 1 is just a plan of the mining face, and current numerical simulation software is two-dimensional, allowing boundary conditions to be set only around the sides. In this case, it is not possible to apply loads at the location where seismic ground pressure occurs. Therefore, the profile of the seismic ground pressure location must be taken for numerical simulation, as shown in Figure 3.

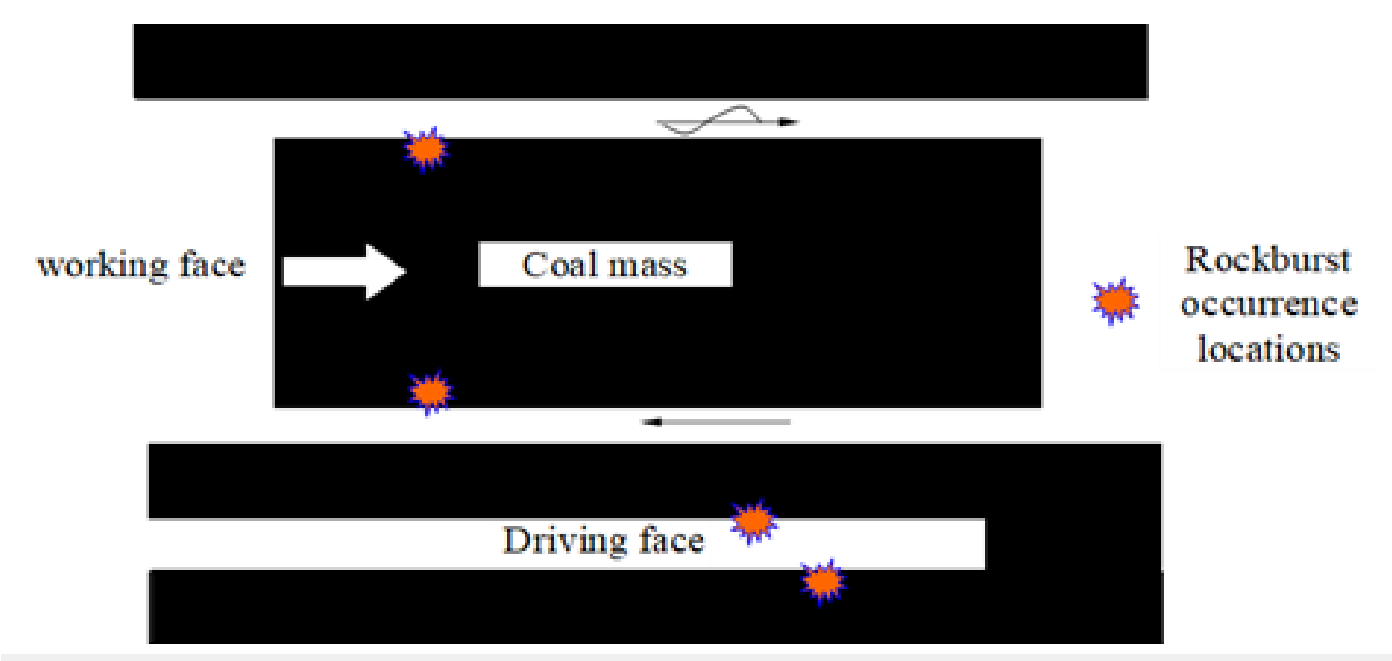


Figure 2: Location of seismic ground pressure numerical simulation object.

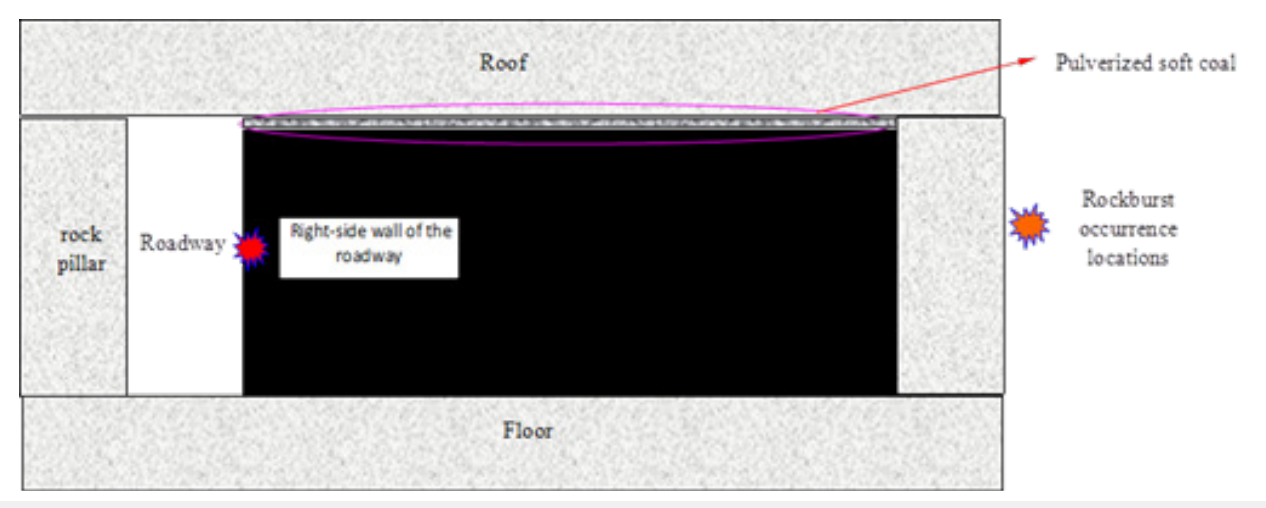


Figure 3: Numerical simulation plan for seismic ground pressure.

Figure 2 is the design diagram of the specific seismic ground pressure numerical simulation plan. The location of seismic ground pressure occurs on the right side of the roadway, which is a large-scale solid coal mass. Seismic ground pressure typically occurs in areas with hard and thick surrounding rock, and there is a thin layer of powdery soft coal (approximately 0.1 to 0.2m thick) between the roof and the coal seam. Therefore, hard roof and floor slabs are set below and above the coal body, and weak coal is placed between the coal seam and the roof.

Based on the above numerical model, in order to investigate the occurrence process of rockbursts at the mining face during excavation, the RFPA2D software was employed to simulate stress distribution. The relevant parameters were set according to the conditions of the 11-2 coal seam at Zhuji Mine and the computational capability of the computer as follows: the average dip angle of the coal seam is 3°, considered as horizontally bedded. The model dimensions are 4m×16m, divided into 20×80 elements, with a coal thickness of 1.2m, soft coal thickness of 0.2m, roof thickness of 1.60m, and floor thickness of 1.0m. The permeability coefficient at the rock boundaries in the model is set to zero, and no gas is present. The gas pressure at the roadway location is atmospheric, approximately 0.1MPa. The coal seam gas pressure is set to 0.5MPa, 1.0MPa, and 1.0MPa, respectively, according to the three experimental schemes. The numerical model uses a plane strain analysis, with stress boundary conditions at the top and

bottom, and displacement boundary conditions on the left and right sides. The displacement boundaries are fixed at zero, while the stress boundaries are set to 20.0MPa, 10.0MPa, and 20.0MPa, respectively, for the three experimental scenarios. The roadway is 1.0m wide, and the coal pillar is 2m wide.

Additionally, the mechanical and seepage parameters of the coal-rock mass are listed in Table 1. This study con-structs a two-dimensional numerical model based on the geological conditions of the 1111(1)-working face at Zhuji Mine in Huainan, fully considering the coal seam dip angle, thickness, and mechanical property differences between overlying and underlying strata to ensure realistic simulation results. The numerical model established with the specified parameters is shown in Figure 4.



Figure 4: Numerical calculation model of seismic ground pressure.

Table 1: Mechanical and permeability parameters of the numerical model.

Material	Homogeneity	Elastic Modulus (GPa)	Compressive Strength (MPa)	Poisson's Ratio	Compression- to-Tension Ratio	Permeability Coefficient (Km²/ (MPa²·d))	Internal Friction Angle (°)	Coupling Coefficient	
Soft Coal	8	5	5	0.3	25	0.05	15	0.2	
Coal Seam	10	10	12	0.3	20	0.1	30	0.2	
Rock Layer	20	50	55	0.25	10	0.01	35	0.1	

AES.000583. 4(2).2025 5

In Figure 4, the entire model is surrounded by rock layers, with the gray area in the middle representing the coal to be excavated. The upper dark gray area is soft coal, simulating the thin layer of powdery soft coal at the top of the coal seam. The black area on the left side of the coal body represents the excavation space, which is the tunnel. After excavation, the soft coal between the coal seam and the roof breaks first, followed by partial coal body rupture near the tunnel. After the initial tunnel is formed, the coal body rupture conditions under the three simulation conditions are basically the same. The black squares inside the coal body in the diagram represent broken failure units.

Numerical simulation of rockburst under high stress and moderate gas pressure conditions

The evolution of coal body fracturing during rockburst development under high stress and moderate gas pressure conditions was obtained through numerical simulation, as shown in Figure 4. According to the figure, as stress increases deep within the coal wall, the soft coal at the top of the coal seam is the first to fail, followed by fracturing in the underlying coal, and finally rupture and failure at the coal seam base. This indicates that the rupture of the top soft coal plays a leading role, intensifying stress concentration in coal units. The self-failure of the coal body causes rapid energy release, generating additional stress and pushing coal masses forward, resulting in large-scale rupture at the bottom and

ultimately triggering a rockburst.

Alongside the coal rupture evolution diagram, the simulation also generated a gas flow distribution map, as shown in Figure 4. In this figure, green arrows represent gas flow, with the direction indicating flow direction and the arrow size indicating gas flow rate. From the distribution of green arrows, it can be seen that gas flow is higher near the coal wall and lower closer to the floor. That is, gas flow is higher near the coal wall and in the top soft coal, although in the numerical model the permeability of soft coal is relatively low, and based on Darcy's law, gas flow should also be low. The reason is likely that after stress-induced fracturing deep within the coal wall, a large amount of gas is instantly de-sorbed. Before a new adsorption equilibrium is established, gas pressure rises sharply. The fine-grained soft coal at the top of the seam is torn or even expelled by high-pressure gas flow, significantly increasing its permeability. Therefore, gas flow in this area is higher than that in the lower coal body.

Numerical simulation of rockburst under moderate stress and high gas pressure conditions

Similarly, by adjusting the model's stress and gas pressure parameters, the evolution of coal fracturing and gas flow distribution during rockburst development under moderate stress and high gas pressure conditions can be obtained, as shown in Figure 5.

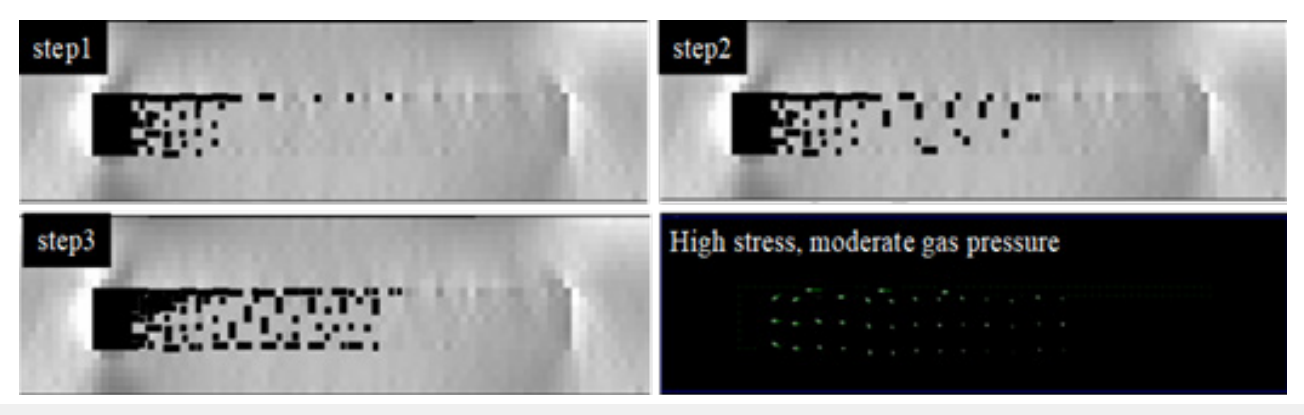


Figure 5: Evolution of coal body rupture under high stress and moderate gas pressure.

Compared with Figure 4, the failure processes under the two conditions are largely similar. The main difference is that under moderate stress and high gas pressure, the range of coal body fracturing is relatively limited. Moreover, there is no large-scale collapse of the upper coal body near the coal wall, as seen in Figure 4. This indicates that rockburst under these conditions is relatively weak, possibly involving only outward bulging of the coal wall without coal ejection. Overall gas flow is relatively high, but flows mainly from the coal body toward the soft coal. This suggests that un-der moderate stress, vertical cracks are more prevalent in the

coal body and are further torn open under high gas pressure.

Numerical simulation of rockburst under combined high stress and gas pressure conditions

In the previous two simulations, either the ground stress or gas pressure was high, while the other was at a moderate level. Now, according to the designed numerical model, a simulation is conducted under conditions of both high ground stress and high gas pressure. The evolution diagram of coal fracturing and gas flow distribution under these conditions is shown in Figure 6.

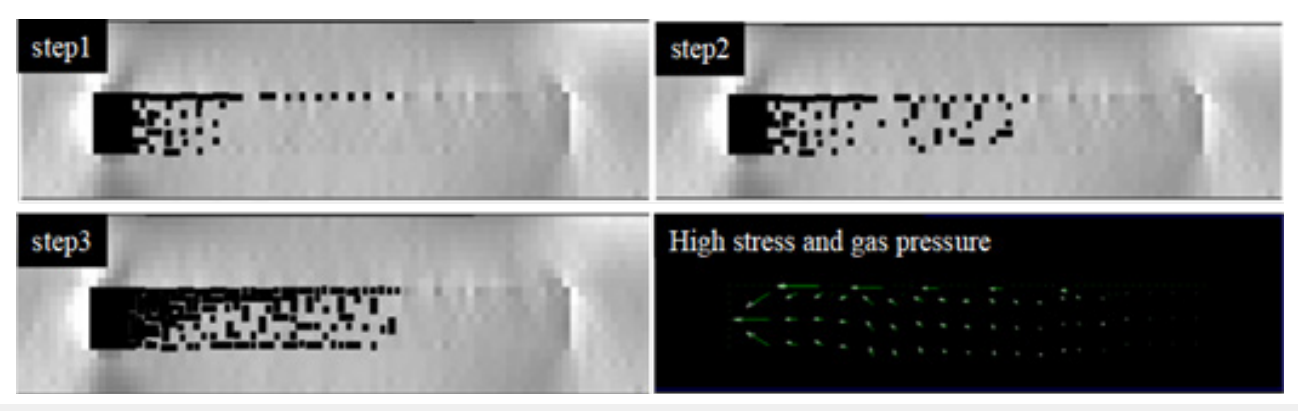


Figure 6: Evolution of coal body rupture under high stress and gas pressure.

Compared with the previous two cases, the fracturing process of coal under high stress and gas pressure conditions is generally similar. The main characteristics of rockburst under these conditions are: under combined high ground stress and gas pressure, the initial rupture of soft coal is more intense, with noticeably smaller spacing between failure units. Large-scale collapse occurs in the upper coal body near the coal wall, indicating that the rockburst is more severe under these conditions. Gas flow is higher than in the other two cases, and the coal wall experiences deeper failure.

Mechanism of Coal Body Impact Movement under the Coupling Effect of High Ground Stress and Gas Pressure

Under different stress and gas pressure conditions, the occurrence of dynamic ground pressure starts with the rupture failure of soft coal at the top deep in the coal wall under stress,

followed by plastic failure of coal in an elastic state under stress. (The presence of gas reduces the strength and elasticity of the coal body, which slows the release rate of elastic strain energy; on the other hand, it aids in stress-induced tearing of the coal body.)

Eventually, the coal body is impacted and ejected under the combined effect of residual elastic strain energy and gas pressure. According to the numerical simulation results, under high stress and gas pressure conditions, the initial rupture of soft coal is relatively violent, and the distance between black damage units is small. Moreover, under the instant release of high-pressure gas in the deep coal body, the powdered coal is carried away by high-pressure airflow, which inevitably causes the stress transfer in the overlying strata to be borne by the smaller, harder coal particles. At this point, the stress distribution under different conditions is shown in Figure 7.

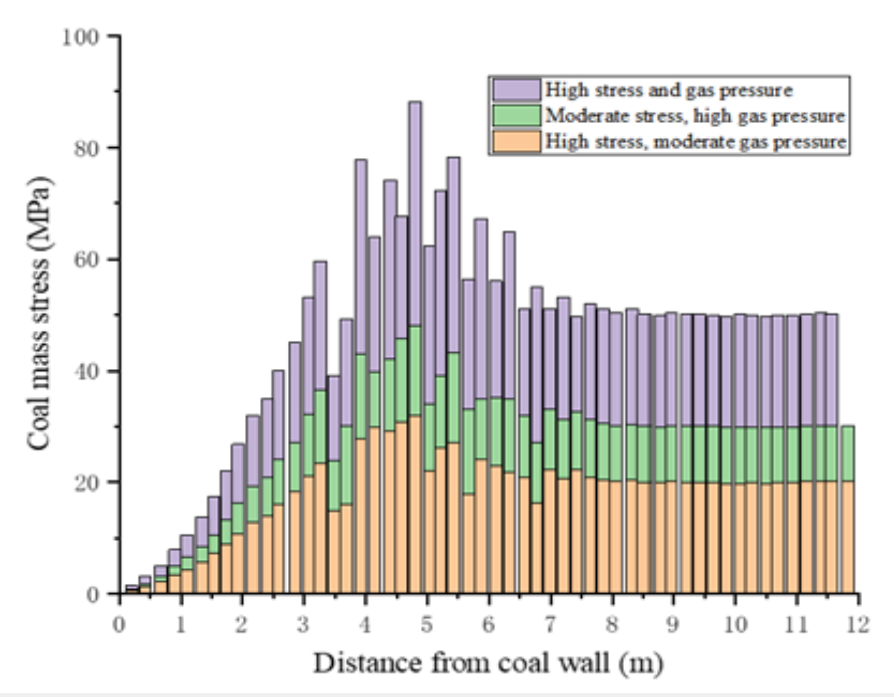


Figure 7: Stress distribution curves of soft coal under different conditions.

AES.000583. 4(2).2025 7

Comprehensive comparative analysis of the three stress distribution curves above shows that the stress concentration factor in the first two conditions is about 1.5, while under high stress and gas pressure conditions, it is about 2.0. This indicates a more intense stress concentration, because under high stress and gas pressure, after the rapid destruction of soft coal at the top of the coal body, the hard coal particles bearing the stress are smaller. Additionally, the high-pressure gas flow may carry away some powdered coal, which makes it more likely to form local stress concentrations, with greater fluctuation. This is consistent with the situation shown in the three stress distribution curves, where the range of stress peaks is relatively wide in the first two conditions, which is the reason for their lower stress concentration. Therefore, it can be considered that before the occurrence of dynamic ground pressure, in the first two conditions, the unbroken coal particles at the top of the soft coal in the coal body can be treated as small fast-moving bodies. During the occurrence of dynamic ground pressure, the impacted coal body slides along with the slider, which is considered sliding friction; while under high stress and gas pressure conditions, due to the smaller size of the unbroken coal particles at the top of the soft coal, it is common knowledge in physics that very small particles may roll during the sliding process. That is, the impacted coal body under these conditions can be considered as rolling friction. As is well known, the rolling friction resistance of an object is much smaller than that of sliding friction, which is why the dynamic ground pressure disaster under high stress and gas pressure conditions is much more severe than in the first two cases. Simultaneously, during the occurrence of dynamic disasters, due to the large area of heat exchange between gas and coal, the heat exchange rate is very fast, and it can be assumed that the temperatures of coal and gas are essentially the same.

Mechanism of Rockburst Triggering under the Coupling of High In-situ Stress and Gas Pressure

Currently, there is extensive research on the mechanisms

of rockburst, but studies specifically addressing the triggering process--particularly under the coupled effect of high in-situ stress and gas pressure--are extremely limited in the open literature.

Mechanism of gas desorption induced by high in-situ stress disturbance

The failure of brittle materials is governed by the presence of internal fractures. Coal, being a naturally heterogeneous material, contains numerous micro-pores and cracks. When saturated with high-pressure gas, stress concentration occurs at crack tips, leading to the initiation of new cracks and eventual coal failure. Cracks in coal are typically of the opening mode, surrounded by isotropic material that behaves as a continuous medium, and the surrounding medium is considered a linear elastic body. The pore walls of coal adsorb gas molecules mainly through intermolecular attraction between coal surface molecules and gas molecules, resulting in a short-term retention of gas molecules on the coal surface. The dominant interaction force between coal and gas molecules is the van der Waals force. Gas molecule desorption primarily relies on energy input through intermolecular collisions or increased temperature.

When the temperature of the coal-gas system rises, the random motion of gas molecules intensifies, increasing collision strength and frequency. This raises the kinetic energy of adsorbed gas molecules, shortens their residence time on the coal surface, and reduces overall gas adsorption. In summary, adsorbed gas molecules are subjected to van der Waals forces from the coal pore surface while simultaneously undergoing random motion with a certain amount of kinetic energy. However, this energy is usually insufficient to overcome the van der Waals force, as illustrated in Figure 8.

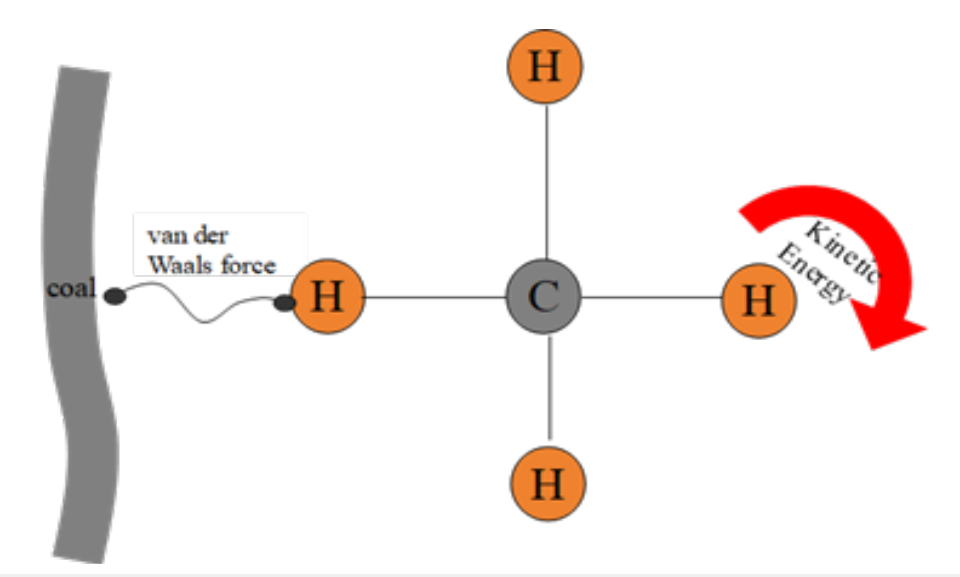


Figure 8: Schematic diagram of force equilibrium of adsorbed gas molecules on the coal wall.

If heated or struck by other free molecules, energy transfer may increase the gas molecule's kinetic energy enough to overcome van der Waals forces and transition into a free molecule. This is analogous to a tethered iron ball in circular motion: the tensile strength of the rope represents van der Waals force, while the ball's kinetic energy mirrors that of a gas molecule. As the ball's speed and energy increase, the rope's tensile force also rises. When it exceeds the rope's strength, the rope breaks and the ball flies off--analogous to a gas molecule escaping adsorption. In other words, whether a gas molecule can escape from the coal wall depends on the relative magnitude between its kinetic energy and the van der Waals forces between the gas molecule and the coal. At the moment of crack formation due to pore rupture in the coal, stress peak transfer causes the coal wall to rapidly rebound and vibrate, similar to the leftward motion of the coal body on the left side of Figure 8, which also drives gas molecules to move leftward.

This exerts a force on the freely oscillating gas molecules in the leftward direction, which in an instant provides them with acceleration to match the coal wall's leftward velocity. Here, the coal wall is the active side applying force, and the gas molecule is passive. Thus, the van der Waals force must not only restrain the molecule's free movement but also resist its leftward acceleration. If insufficient, the gas molecule will detach from the coal wall during the leftward motion and become free. Based on the previous analysis, the displacement of the coal wall varies at different positions of the ellipse, so the required acceleration force within the same time frame also differs. Therefore, the proportion of gas molecules escaping the van der Waals forces also varies. Assume the van der Waals force between the coal wall and gas molecules is f, the stress from the molecule's free motion is F₁, and the additional stress due to the coal wall's instantaneous displacement is F2, Then, the stress condition for gas molecules to escape the coal wall is:

$$f \le F_1 + F_2$$
 (1)

When both sides of equation (1) are equal, it represents a critical state. According to Newton's law, we have:

$$L_1 - L = \frac{1}{2} \frac{F_2}{m} t^2$$
 (2)

 $L_1-L=\frac{1}{2}\frac{F_2}{m}t^2 \ (2)$ In the equation, m is the mass of the gas molecule and t is time.

Transforming the above equation yields:

$$F_2 = \frac{2m(L_1 - L)}{t^2} \ (3)$$

Combining equations (1) and (3), we get:

$$\frac{2m(L_1 - L)}{t^2} \ge f - F_1$$
 (4)

According to equation (4), whether a gas molecule on the coal pore wall can desorb at the moment of coal wall rupture and vibration depends mainly on several factors: the larger the coal wall's vibration displacement and the greater the gas molecule's mass, the higher the probability of desorption; the more intense (i.e., shorter in time) the vibration, the greater the chance of desorption.

In summary, the better the coal's elasticity, the greater its compressive deformation under the same stress (i.e., larger L,-L); the higher the ground stress, the more intense the redistribution of stress due to mining activity (i.e., smaller t); Under such conditions, the probability of adsorbed gas molecules desorbing from the coal wall increases; once the molecules become free, the pore gas pressure rises, which can easily induce coal-rock dynamic disasters such as out-bursts.

Mechanism of coal body instability under coupled high ground stress and gas pressure

Distribution of coal stress and gas pressure ahead of the mining face

Generally, ahead of the mining face, based on ground stress distribution, the area can be divided into the pressure relief zone, the stress concentration zone, and the original stress zone, as shown in Figure 9. In Figure 9, r represents the distance from the excavation face, σ is the ground stress, and σ_0 is the original stress. The zone from 0 to R_1 is the pressure-relief zone, where the stress is lower than the original rock stress. The zone from R₁ to R₂ is the stress concentration zone, where stress is higher than the original rock stress; it can be subdivided into a plastic deformation zone (R_1-R_p) and an elastic deformation zone (R_p-R_2) . The zone from R_2 to ∞ is the original stress zone, where the stress equals the original

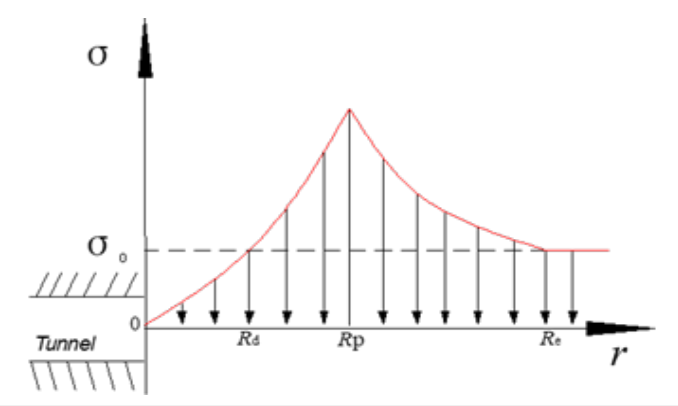


Figure 9: Stress distribution in the coal body ahead of the working face.

Copyright © Kaiwen Zhang Academic J Eng Stud

Within the range of 0 to $R_{p'}$, the stress ahead of the excavation face can be expressed by Equation (5).

$$\sigma = \frac{0.1 + K\cot\varphi}{1 - A_1} [\frac{1 + \sin\varphi}{1 - \sin\varphi} (\frac{r}{R_0})^{\frac{4\sin\varphi}{1 - \sin\varphi}} - 1] + \frac{0.1 - pA_1}{1 - A_1} \ \, \text{(5)}$$
 In this equation: K -- cohesion (MPa); φ -- internal friction angle

In this equation: K -- cohesion (MPa); φ -- internal friction angle of the coal seam (rad); n -- porosity; R_0 --road-way radius (m); p -- gas pressure (MPa).

In Equation (5), when r=Rp, then $\sigma=k\sigma_0$, where k is the stress concentration factor. By transforming Equation (5), Equation (6) is obtained:

$$R_{p} = R_{0} \left(\left(\frac{k(1 - A_{1})\sigma_{0} - 0.1 + pA_{1}}{0.1 + k \cot \varphi} + \right) \frac{1 - \sin \varphi}{1 + \sin \varphi} \right)^{\frac{1 - \sin \varphi}{4 \sin \varphi}}$$
(6)

The gas pressure acting ahead of the roadway can be expressed as: $P=n\sqrt{\frac{2E}{b}(1-e^{-bx})}$, where P is the gas pressure at a point ahead of the

roadway, n and E are expressions, with n approximately equal to the porosity, b is a constant, and x is the distance from the coal wall. The above expression can be simplified to: $P = P_1 \sqrt{(1 - e^{-bx})}$, where P_1 is the original gas pressure of the coal seam.

Based on the above gas pressure expression and different parameter settings, the gas pressure curves can be derived as shown in Figure 10. In Figure 10, the horizontal axis represents the distance from the borehole wall (m), and the vertical axis represents gas pressure (MPa). The original gas pressure is set to 0.8 MPa and b_1 is taken as 150. The three curves correspond to the gas pressure distributions at 1 minute, 31 minutes, and 61 minutes, respectively. It is clearly shown in the figure that gas pressure increases exponentially with distance from the coal wall, up to the original coal seam gas pressure.

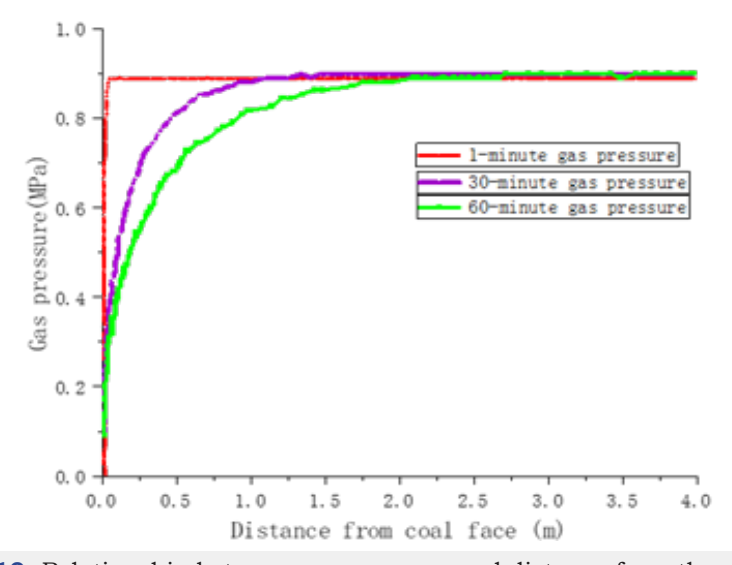


Figure 10: Relationship between gas pressure and distance from the coal wall.

 Analysis of the instability mechanism of coal ahead of the working face

Based on the stress and gas pressure distribution in front of the working face, it is known that the stress initially increases, then decreases and stabilizes, while the gas pressure gradually increases and eventually stabilizes. Under stress concentration in front of the working face, the coal fractures and transitions from an elastic to a plastic state, during which a large volume of high-pressure gas desorbs. The airflow enters the upper part of the coal seam through fractures, and the weak fragmented coal between the seam and the roof is expelled outward under the action of high-pressure gas. A small amount of hard coal particles is left between the roof and the coal seam, as shown in Figure 11.

In the deep part of the working face, as the coal transitions from an elastic to a plastic state, its elastic deformation energy must be released. The magnitude of this energy depends directly on the impact energy index, and the release rate is determined by the dynamic failure duration. Therefore, the energy released per unit time depends on the relative values of these two indicators. The greater the energy released per unit time, the higher the induced additional stress. Since coal is not a rigid body, this energy will propagate toward the working face in the form of stress waves. As the stress wave propagates toward the working face, the coal along its path absorbs part of the energy and undergoes deformation under the disturbance. The energy consumed in deformation and instability of the coal in front of the working face varies under different stress and gas pressure conditions. A unit of coal adjacent to the coal wall of the working face may undergo bending deformation or even collapse under the influence of stress waves. This manifests macroscopically as the occurrence of a rockburst. Each coal unit under the influence of a stress wave can be simplified mechanically as a body subjected to lateral forces, with the lower end fixed and a certain shear resistance. Its upper end contacts the roof via a spherical coal block, and their relative motion is characterized by rolling friction.

Triggering mechanism of rockbursts under coupled high ground stress and gas pressure

A coal unit within the stress limit zone in Figure 11 is selected for two-dimensional planar force analysis, as illustrated in Figure 12. In Figure 12, represents the stress acting perpendicular to the

impact direction (MPa). Based on fundamental rock mechanics, this stress in the stress limit zone increases approximately exponentially and can be expressed as:

$$\sigma_{v} = \sigma_{b_{1}} e^{b_{1}x} (7)$$

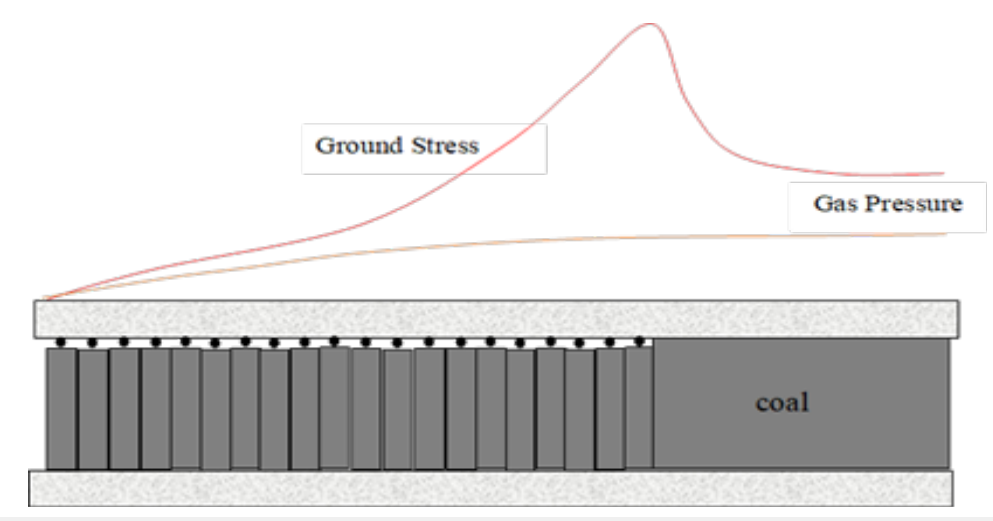


Figure 11: Structural diagram of the coal-rock body before rockburst occurrence.

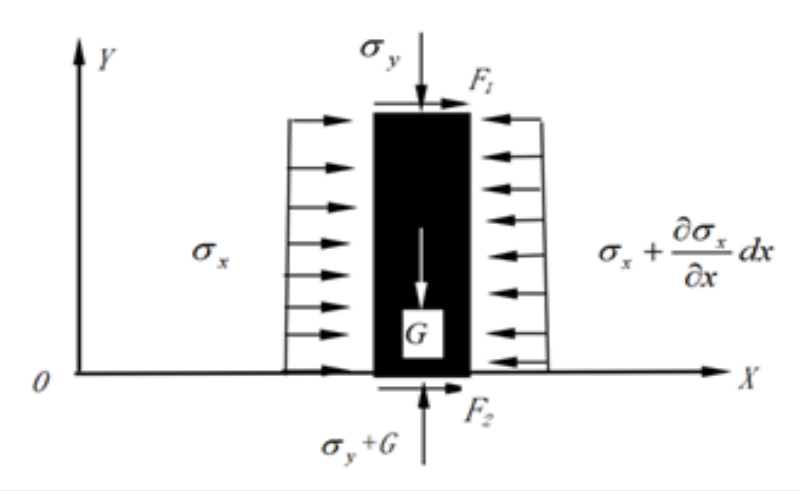


Figure 12: Schematic diagram of stress on coal in the stress limit zone.

In Equation (7), σ_{b_1} is the compressive stress at the coal wall of the roadway (MPa), b_1 is a coefficient describing the stress variation rate (m⁻¹), and x is the depth from the coal wall (m). G is the self-weight stress of the analyzed coal body (MPa); F_1 is the frictional resistance between the coal seam and roof (rolling friction, MPa); F_2 is the frictional resistance between the coal seam and floor (sliding friction, MPa); σ_x is the stress parallel to the impact direction, which is correlated with σ_y .

Under normal conditions, the system is in equilibrium, and the frictional resistance at the top and bottom may be below their maximum values. When elastic energy from coal failure and expansion energy from gas desorption are released, they act on the coal body as compressive disturbances in the form of elastic waves, effectively increasing the ap-plied stress, whose maximum value is denoted as. Under the stress of the elastic wave, the coal body undergoes compressive deformation and moves toward the excavated roadway space (displacement along the Y-direction may vary; if top and bottom frictional resistance is large, displacement may occur only in the central part).

Thus, based on whether frictional resistance at the top and bottom reaches its limit, coal burst modes can be categorized into three types: (1) both resistances below maximum--no movement at top or bottom; (2) top reaches maximum but bottom does not--top moves while bottom remains stationary; (3) both reach limit--top and bottom both move.

Under high ground stress and gas pressure, the energy triggering rockbursts originates from the coal-rock body's elastic strain energy and gas expansion energy. Under triaxial stress, the elastic strain energy of the coal-rock mass can be expressed as follows:

$$W_{t} = \frac{1}{2E} (\sigma_{1}^{2} + \sigma_{2}^{2} + \sigma_{3}^{2} - 2\mu(\sigma_{1}\sigma_{2} + \sigma_{2}\sigma_{3} + \sigma_{1}\sigma_{3}))$$
(8)

In Equation (8), W_t is the elastic strain energy of the coalrock body (MJ/m³); σ_1 , σ_2 , σ_3 are the principal stresses in three directions (MPa); and μ is the Poisson's ratio of coal.

At the Zhujiming 1111(1) working face and 1112(1) transport roadways, the vertical stress is 19MPa, the maximum horizontal stress is 22MPa, and the minimum is 17MPa; the Poisson's ratio of coal is approximately 0.3 and its elastic modulus is about 500MPa. Using Equation (8), the elastic strain energy of the coal-rock body can be calculated as:

$$W_{_{\ell}} = \frac{1}{2 \times 500} (19^2 + 22^2 + 17^2 - 2 \times 0.3 \times (19 \times 17 + 17 \times 22 + 19 \times 22)) = 0.465 MJ \ / \ m^3 \ .$$

In the context of dynamic disasters such as coal and gas outbursts or rockbursts, whether heat exchange occurs remains a subject of academic debate. One view holds that the entire dynamic disaster process occurs over a very short duration, typically around 40 seconds; The two participating media--coal and gas--have very low thermal conductivity: 0.16kcal/(m·h·°C) for coal, and 0.026 and 0.013kcal/(m·h·°C) for methane and carbon dioxide, respectively. Therefore, the amount of heat exchanged between coal and gas in such a short time is negligible, and the process can be considered adiabatic. Another view suggests that during a dynamic disaster, the contact area for heat exchange between gas and coal is extensive, resulting in rapid heat transfer. As such, the temperatures of coal and gas can be considered nearly equal, and gas expansion work must absorb substantial heat from the coal. In other words, the gas expansion process during dynamic disasters is not adiabatic but rather a polytropic process.

Based on these two perspectives, different formulas for calculating gas expansion energy have been de-rived. However, issues remain: the adiabatic analysis does not consider heat transfer, and more critically, it neglects the adsorption characteristics of gas. That is, it treats adsorbed and free gas as a single entity. Although the non-adiabatic analysis considers heat transfer and distinguishes between adsorbed and free gas, it suffers from large calculation errors in the gas content-pressure relationship at low pressures due to pressure variability.

A. Temperature Variation Analysis During the Occurrence of Dynamic Disasters

The main causes of coal temperature reduction during coal-rock dynamic disasters are gas expansion and gas desorption from coal. Using an infrared thermometer, the temperature variation of coal induced by gas desorption was measured, showing a range of 0.81 to 6.26 °C. In conjunction with measurements of temperature

changes during coal and gas outbursts, the observed temperature variation ranged from 0.7 to 1.6 °C. During the gas desorption process, the coal temperature changed by 1.8 to 5.6 °C as a result of gas release. These results indicate that temperature changes during dynamic disasters are minimal and the process can be regarded as approximately isothermal. Therefore, in analyzing gas expansion energy, the temperature change can be neglected to simplify calculations.

B. Theoretical Analysis of Gas Expansion Energy

Coalbed gas content refers to the amount of gas contained per unit mass of coal, existing in two forms: free gas and adsorbed gas. The total gas content in coal seams is the sum of both, and the calculation formula is given in Equation (9).

$$X = \frac{V_1 p_1 T_0}{T_1 p_0 \xi} + \frac{abp_1}{1 + bp_1} e^{n(t_0 - t_1)} \frac{100 - A - W}{100 \times (1 + 0.31W)}$$
(9) In the formula, V1 represents the pore volume of the combustible

In the formula, V1 represents the pore volume of the combustible substance in the unit weight of coal, $m^3/t.r$; p_1 represents the gas pressure, MPa; T_0 represents the absolute temperature under standard conditions (273K); p_0 represents the standard atmospheric pressure; T_1 represents the absolute temperature of coal seam gas, K; ξ represents the gas compression coefficient; e is the base of the logarithm for spontaneous combustion; t_0 is the temperature when the coal adsorption constant is determined in the laboratory, °C; t1 is the temperature of the coal seam, °C; e0; e1 is the coefficient; e2, e3 are the coal adsorption constants, e3/t, MPa^-1; A, W are the air-dried ash content and air-dried moisture content of coal, in percentage; X is the combustible gas content in coal, e3/t.r.

A series of integrations on equation (1) are performed, leading to the following formula:

wing formula:

$$E = (V_{1}p_{1} + e^{n(t_{0}-t_{1})} \frac{100 - A - W}{100(1 + 0.31W)} \frac{T_{1}P_{0}\xi}{T_{0}} \frac{abp_{1}}{1 + bp_{1}}) (10)$$

$$\ln(\frac{p_{1}}{p_{0}}) + e^{n(t_{0}-t_{1})} \frac{100 - A - W}{100(1 + 0.31W)}$$

$$\frac{T_{1}P_{0}\xi}{T_{0}} ab(\frac{1}{1 + bp_{0}} - \frac{1}{1 + bp_{1}} + \ln(\frac{1 + bp_{0}}{1 + bp_{1}}))$$

Equation (10) is the theoretical calculation formula for gas expansion energy, where the independent variables are gas pressure and gas content.

The calculation formulas for gas expansion energy (9) are quite complex, making it difficult to directly distinguish the relationship between them. Therefore, first, based on the coal seam gas parameters measured in the ZHUJI Mine 1111(1) mining face and 1112(1) transport tunnel, the basic parameters for calculation are determined, as shown in Table 2; then, using Equation 1, computergenerated graphs showing the relationship curves between gas expansion energy, gas pressure, and gas content are drawn, as shown in Figure 13 & 14. From Figure 13 & 14, it can be clearly seen that as pressure or content increases, gas expansion energy gradually increases, but its rate of increase slows with rising pressure, while it increases more rapidly with rising content.

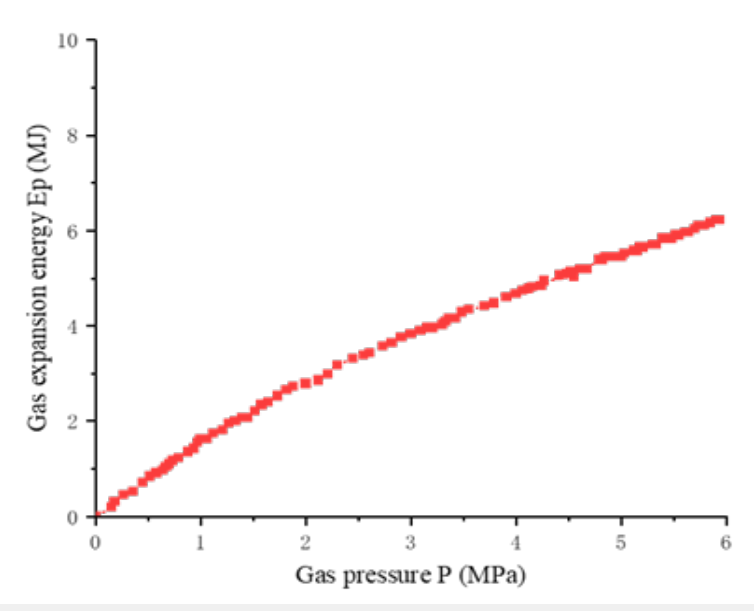


Figure 13: Curve of gas expansion energy versus pressure.

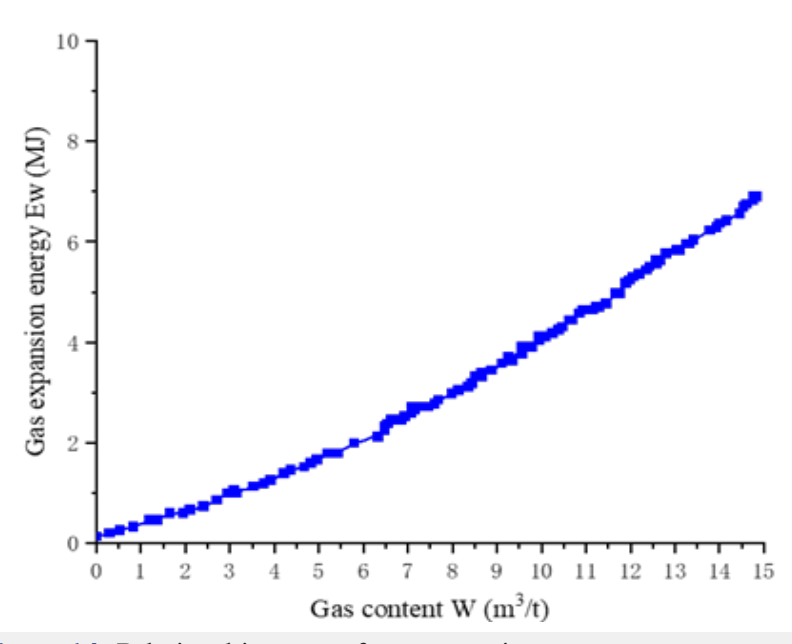


Figure 14: Relationship curve of gas expansion energy versus content.

Table 2: Main parameters of the coal body.

Parameters	T0	T1	ξ	a	b	P ₀	n	t _o	t1	A	W	V1
	(K)	(K)		(m^3/t)	(MPa ⁻¹)	(MPa)		(°C)	(°C)	(%)	(%)	(m³/t.r)
Value	273	300	1.1	16	0.5	0.1	0.02	30	27	20	1.6	0.09

The maximum gas pressure at the ZHUJI Mine 1111(1) mining face and 1112(1) transport tunnel is 0.51 MPa, the maximum gas content is $3.86 m^3/t$, and the gas expansion energy is approximately 0.64 MJ/t. Assuming a coal bulk density of 1.4, the gas expansion energy per unit volume of coal is 0.89 MJ, which is higher than the elastic deformation energy of the coal rock $(0.465 MJ/m^3)$.

Additionally, according to the mine's outburst identification report, the highest gas pressure at around the 901m elevation of the ZHUJI Mine 11-2 coal seam is approximately 1MPa, giving a gas expansion energy of about 1.43MJ/t. When converted to gas expansion energy per unit volume of coal, this is 2.0MJ, which is much higher than the elastic deformation energy of the coal rock.

Therefore, it can be seen that when gas pressure is relatively low, the energy for dynamic disasters originates from the elastic deformation energy of the coal rock and the gas expansion energy, with little difference between the two. Un-der conditions of high ground stress and gas pressure, the gas expansion energy is much higher than the elastic deformation energy of the coal rock and becomes the main energy source for dynamic disasters. The release of these two types of energy manifests macroscopically as a force acting on the coal body, causing deformation or even overall movement. Under these conditions, the main type of dynamic pressure occurs in the third mode, where both the top and bottom of the coal body experience movement. This is because the energy required for the third mode of dynamic pressure is much higher than the elastic deformation energy of the coal rock. From an energy perspective, relying solely on high ground stress is insufficient, while high-pressure gas expansion energy is significantly higher than the energy consumption of the first two types of dynamic pressure.

Conclusion

- a. Among the three simulated conditions, rockbursts were most intense under the coupled high ground stress and high gas pressure scenario. Initial fracturing of soft coal occurred earlier, the spacing between failure units decreased by 62%, and large-scale collapse occurred in the upper part of the coal wall. The gas flow rate increased by more than 40% compared to single-factor conditions, indicating that gas acted as a "combustion promoter" during the impact process.
- b. Rockburst disaster mechanism: (i) Intensified stress concentration--residual hard coal fragments led to a local stress concentration factor as high as 2.0, significantly greater than 1.5 under single-factor conditions; (ii) Enhanced gas drag effect--gas desorption generated high-pressure airflow that tore soft coal apart, carried away debris, and formed open pathways, facilitating rapid energy release; (iii) Frictional mode transition--the coal body transitioned from sliding to rolling friction, reducing frictional resistance by 38%, and significantly increasing impact kinetic energy.
- c. Energy-driving mechanisms triggering rockbursts: (i) Synergistic release of elastic energy and gas expansion energy constitutes the primary source of rockburst energy; (ii) Gas expansion energy increases exponentially with gas con-tent and serves as a key driving force for high-velocity ejection; (iii) Energy conversion efficiency peaks under coupled high-stress and high-gas conditions, significantly enhancing impact failure potential.
- d. The study clarifies the triggering mechanism of rockbursts under coupled high ground stress and high gas pressure and reveals the critical conditions for energy accumulation and release. The proposed ground stress-gas pressure coupling model provides new insights for predicting and controlling dynamic disasters in deep coal mines. It is recommended that future work integrate field monitoring data with multi-field

coupling early warning models to enhance the scientific and precise prevention of rockbursts.

References

- Yuan L, Wu JS, Yang K (2023) Key technologies and applications of intelligent precise coal safety mining. Journal of Mining and Safety Engineering 40(5): 861-868.
- Yuan L (2023) Theoretical and technological considerations for the highquality development of China's coal-dominant energy security. Bulletin of Chinese Academy of Sciences 38(1): 11-22.
- Lu J, Yin GZ, Gao H (2020) Experimental study on compound dynamic disasters and pressure relief drilling of gas-bearing coal under true triaxial loading conditions. Journal of China Coal Society 45(5): 1812-1823.
- Zhu ZH, Sun FY, Guo JQ (2023) Study on rockburst tendency of deep underground engineering based on multi-factor influence. Electronic Journal of Structural Engineering 23(1): 1-12.
- Lu A, Yan P, Lu W, Ming C, Gaohui W (2021) Numerical simulation on energy concentration and release process of strain rockburst. KSCE Journal of Civil Engineering 25(10): 3835-3842.
- Pan YS, Song YM, Liu J (2023) Patterns, transitions, and new frontiers in coal burst prevention and control in China. Chinese Journal of Rock Mechanics and Engineering 42(9): 2081-2095.
- Lai XP, Jia C, Xu HD, Feng C, Xudong L. et al. (2024) Precursor characteristics and disaster prevention of rockburst in steeply inclined deep ultra-thick coal seams. Journal of China Coal Society 49(1): 337-350.
- Liu WC, Zhao YX (2023) Catastrophic mechanism and prevention of rockburst in typical working faces of Hongqinghe Mine. Journal of Mining Science and Technology 8(6): 803-816.
- 9. Cui F, Zhang TH (2021) Triggering mechanism and time window effect of solar-lunar tidal forces on rockburst. Chinese Journal of Rock Mechanics and Engineering 40(S2): 3107-3117.
- Askaripour M, Saeidi A, Rouleau A, Mercier-Langevin P (2022) Rockburst in underground excavations: A review of mechanism, classification, and prediction methods. Underground Space 7(4): 577-607.
- Pan JF, Kang HP, Yan YD, Xiaohui MA, Wentao MA, et al. (2023) Method, mechanism, and application of "Artificial Liberated Layer" in roof for rockburst prevention. Journal of China Coal Society 48(2): 636-648.
- Pan JF, Liu SH, Ma WT (2024) Occurrence patterns and classified prevention of rockburst in Shaanxi coal mines. Coal Science and Technology 52(1): 95-105.
- Pan JF, Liu SH, Gao JM (2020) Theory and technology for dynamic-static load separation control of rockburst in deep roadways. Journal of China Coal Society 45(5): 1607-1613.
- Dou LM, Zhou KY, Song SK (2021) Research on mechanism, monitoring, and prevention of coal mine rockburst. Journal of Engineering Geology 29(4): 917-932.
- 15. Dai J, Gong F, Qi S (2023) Quantitative evaluation of rockburst proneness for surrounding rocks considering combined effects of the structural plane and excavation disturbance. Tunnelling and Underground Space Technology 140: 105335.
- Zhang Y, Xia Y, Lin M (2025) Mechanical characteristics and acoustic emission in rockburst under gradient loading on structural planes: An experimental study. Engineering Fracture Mechanics 325: 111297.
- 17. Wang GF, Dou LM, Cai W (2018) Unstable energy triggering mechanism of rockburst. Journal of China University of Mining and Technology 47(1): 190-196.

- 18. Guo W, Liu XQ, Chen L (2024) Targeted monitoring, early warning, and prevention practices for rockburst. Coal Technology 43(2): 171-175.
- 19. Ding ZW, Jia JD, Tang QB (2022) Mechanical properties and energy damage evolution characteristics of coal under cyclic loading and unloading. Rock Mechanics and Rock Engineering 55(8): 4765-4781.